Effect of Reservoir-Subbottom Energy Absorption on Hydrodynamic Forces on Dams

by

Robert L. Hall*, Luis de Béjar*, Keith j. Sjostrom* and Enrique E. Matheu*

ABSTRACT

This paper will summarize the recent experimental programs conducted in the U.S. and China to measure the reservoir-bottom reflection coefficient, α. Theoretical studies will also be presented demonstrating the impacts of the subbottom absorption on the hydrodynamic loads on the upstream face of a concrete dam. The seismic evaluation of the Folsom Dam will be used to demonstrate the impact of including the effect of reservoir bottom absorption on the stresses of a concrete gravity dam.

1. BACKGROUND

The interaction between the dam, the reservoir subbottom, and the reservoir significantly affects the structural stresses in concrete dams when subjected to strong earthquake ground motions. (Hall and Chopra 1980; Fenves and Chopra 1984; Lofti, Roesset, and Tassoulas 1987). The hydrodynamic pressure waves impinging on the reservoir subbottom are partially reflected back into the reservoir and partially absorbed by the reservoir-bottom materials. The absorption of the pressure wave reduces the hydrodynamic pressures on the upstream face of the dam. The absorption of the pressure wave into the materials on the bottom of the reservoir is modeled by a reflection coefficient known as "α." Approximate analytical studies including the effects of this complex interaction demonstrate that the structural responses of concrete dams are strongly sensitive to the amount of energy absorbed by the reservoir bottom materials (Fenves and Chopra 1984; Fok, Hall, and Chopra 1986; Hall, Woodson and Nau 1987; Duron and Hall 1988).

Refraction and reflection procedures have been used to characterize material on the reservoir bottom (Ghanaat, et al. 1993; Ghanaat and Redpath 1995). These procedures were used at seven concrete dam sites in the United States and at the Dongjiang Dam, China. A seismic blasting cap was used to generate a hydrodynamic pressure wave for these experiments, and provided the first step toward determining average values to be used for current numerical procedures for modeling the reservoir-bottom absorption.

A more comprehensive waterborne seismic reflection investigation was performed at Pine Flat Lake, California. The objective of the geophysical investigation was to delineate the geologic stratigraphy and provide acoustic impedance versus depth plots to depths of 30 to 60 meters below the bottom surface upstream of the Pine Flat Dam. The results are intended to be used as input toward the development of seismic modeling algorithms of the Pine Flat Dam and reservoir. The study is also conducted, in part, to compare with the reflection coefficient value computed for the bottom sediments determined from a previous investigation (see Ghanaat and Redpath 1995) using a blasting cap for the generation of a pressure wave.

The current numerical procedures model the reservoir-bottom absorption as a boundary condition, approximating the reservoir-subbottom interaction by a one-dimensional (1-D) wave propagation model with a single parameter, the reflection coefficient, α (Hall and Fenves 1980). This procedure has been implemented into the two-dimensional (2-D)

* U.S. Army Engineer Waterways Experiment Station, Vicksburg, MS

code, EAGD (Fenves and Chopra 1984), for concrete gravity dams and into a three-dimensional (3-D) code, EACD, for arch dams (Fok, Hall, and Chopra 1986). Numerical procedures such as the Boundary Element Method (de Béjar 1996) can be used to model the reservoir-subbottom interaction, accounting for the spatial variation of material properties. Further, models will need to be developed to accurately reproduce the measured response of an actual concrete dam-reservoir-foundation system.

2. MEASUREMENTS

Acoustic subbottom reflections are produced when a source of acoustic energy is deployed just below the water surface and fired. In a homogeneous medium, the acoustic waves extend uniformly in all directions from the source in which the advancing wavefronts are spherical surfaces centered at the source and normal to the direction of propagation. When the acoustic energy arrives at a boundary between two materials of differing density and elastic velocity, part of the energy will be reflected back towards the surface and part transmitted downward into the medium below. Portions of the transmitted energy will also undergo absorption or attenuation in the material while the wavefront propagates through to the next stratigraphic boundary.

The amplitudes of the incident, reflected, and transmitted wave energies vary with respect to the density and velocity of the materials through which the wave energy is propagating. The ratio between the amplitudes of incident and reflected wave energy is called the reflection coefficient (α) and is defined as:

$$\alpha = \frac{A_R}{A_I}$$

where A_R and A_I are the amplitudes of the reflected and incident wave energy, respectively (Telford, et al. 1976). Reflected wave energies are detected using hydrophones or piezoelectric transducers which convert changes in water pressure caused by the acoustic wavefronts into electrical impulses. The electrical signals are amplified, filtered, and recorded using a shallow seismic, digital data acquisition system.

Two independent geophysical techniques for determining α in-situ were used at seven concrete dam sites in the United States and at the Dongjiang Dam, China (Fig 1). The seismic reflection technique measures the incident and reflected shock waves generated by a blasting cap on the reservoir bottom. The seismic refraction technique measures the propagation velocity of the pressure wave in the subbottom materials by measuring the refracted waves and then computing the ratio of the acoustic impedances of the material. The refraction experiments were based on a technique developed by Hunter and Pullan (1990). Blasting caps serve as the source for the generation of a pressure wave for both types of experiments. The α value is computed from the ratio of the acoustic impedances of the reservoir-bottom material and the water in the reservoir (Ghanaat and Redpath 1995).

At the Dongjiang Dam, the reflection experiments were conducted above a submerged concrete cofferdam. The location of the cofferdam was determined during the processing of the experimental data when construction drawing became available. Analyses of the reflection experiments resulted in a completed α value of 0.63 for the reservoir-bottom sediments. This value was affected by the cofferdam. The results from the seismic refraction testing determined α to be 0.40 for the reservoir-bottom sediments and 0.80 for the granite rock (Ghanaat et al. 1993).

At the seven U.S. dam sites, the values of α for the reservoir-subbottom material varied over a range from -0.55 to 0.66. Pine Flat, Hoover, and Folsom had negative α values. The negative values are the result of the wave propagation velocity through the reservoir-bottom material being less than the propagation velocity through water. This can occur when the density of the material is less than that of water. This leads to

the conclusion that the reservoir-bottom material may contain decaying organic material which is producing gases in the material. Glen Canyon had a low α values of 0.15. Monticello, Morrow Point, and Crystal had α values greater than 0.66. This study concluded that conducting both refraction and reflection experiments is essential for determining α (Ghanaat and Redpath 1995).

A waterborne seismic reflection investigation was also performed in Pine Flat Lake. This study concentrated in the narrow neck of the reservoir upstream of the dam structure. The survey was conducted aboard the WES Research Vessel (R/V) *Waterways Explorer* with acoustic energy generated by two high-resolution subbottom profiling systems. The first system was operated at a frequency of 3.5 and 7.0 kHz and is typically called a 'pinger' because of the audible noise it makes during operation. The second system is a lower frequency 'boomer' system and hydrophone which has an output frequency range of 0.5 to 2.0 kHz to interrogate the subbottom sediment structure. The higher operating frequency of the 'pinger' system allows greater resolution of the bottom and subbottom stratigraphy than the 'boomer' or air gun systems but shallower depths of energy penetration depending on the characteristics of the subbottom material.

The pinger system consisted of a Datasonics SBP-5000 subbottom profiling system. The SBP-5000 transmitters were mounted within a towfish rigidly attached to a telescoping arm and deployed through the front deck of the *Waterways Explorer*. The system allows the transmission of variable-length acoustic pulses (0.2 - 3 msec) over frequency ranges of 3.5, 7.0, 10.0 kHz. The transducers of both the source and receiver were positioned 3 feet below the water surface during data collection. For the Pine Flat Lake study, the length of the pinger pulse width at frequencies of 3.5 and 7.0 kHz was set at 0.2 msec and is typically able to resolve stratigraphic layers having thicknesses greater than or equal to 0.6 meters. A total trace length of 700 samples were digitally acquired every 42 μsec which corresponds to a sampling rate of 16 samples/μsec. This sampling rate provides an effective depth of subsurface exploration of approximately 4.5 to 12.4 meters below the bottom surface, depending on the bottom and subbottom sediment characteristics.

The electro-mechanical source of the boomer system is mounted on a sled and, along with the hydrophone array, towed approximately 21.3 meters behind the R/V during the investigation. The EG&G Models 231 and 232 sources were operated in the frequency range of 0.5 to 2.0 kHz at an energy level of 300 joules. The length of the boomer pulse width at the central frequency of 1.2 kHz is typically able to resolve lithologic layers having thicknesses greater than 1.5 meters. Under typical surveying conditions, a total seismic trace length of 700 samples were collected every 88 μsec (sampling rate = 8 samples/μsec), resulting in exploration depths in excess of 30 meters below the bottom surface.

These detailed studies confirmed the existence of negative values of α as reported by Ghanaat and Redpath in their studies. This study also provided the spacial variation of the reservoir-bottom materials, as well as the depth, of different subbottom material layers. As detailed numerical procedures are developed, this detailed description of the reservoir subbottom may be needed.

3. THEORETICAL SUBBOTTOM-RESERVOIR-DAM INTERACTION EFFECT

The effect of the interaction between the absorptive boundary and the dam via the pressure field transmitted by the fluid medium becomes apparent by considering the simple example in Figure 2. This 2-D model represents the longitudinal section of a reservoir with aspect ratio 3 (the ratio of the reservoir length to the dam height, at full capacity). The water is assumed impounded by a rigid boundary at the far end of the reservoir, and the bottom is characterized by a reflection coefficient typical of a solid continuum [$\alpha \varepsilon (0,1)$].

The system is subjected to a steady-state harmonic acceleration applied uniformly at the rock base, with amplitude 0.30g (where g is the acceleration of gravity), and frequency of 1.0 Hz. Figure 3 indicates the linear distribution of the hydrostatic pressure on the upstream face of the dam, normalized with respect to its value at the bottom. By comparison, the corresponding amplitude of the hydrodynamic pressure field on this front wall is computed at six nodes uniformly spaced along the wall height. These hydrodynamic pressures were estimated using Westergaard's approximation (Westergaard 1933) and appear in Figure 3 normalized with respect to the corresponding hydrostatic pressure at the point under consideration. Notice that the maximum value of the hydrostatic pressure on the wall takes place at node 13, located at a distance of 0.40 H from the bottom, where H is the dam height. At node 13, the hydrostatic pressure is increased by a hydrodynamic pressure with amplitude 33% of the hydrostatic pressure at this node.

The effect of the dynamic interaction between the flexible subbottom and the dam (H = 91.4 meters) is considered at nodes 13, 17, and 21, within the lower 40% of the wall height, where the hydrodynamic contribution to the total pressure field is significant. Figures 4, 5, and 6 show the normalized amplitudes of the hydrodynamic pressure at the nodes in question. The corresponding abscissas in these figures are normalized with respect to the fundamental natural frequency of the impounded water, given by

$$\omega_1 = \frac{C}{4H} \quad [Hz]$$

where C is the velocity of propagation of the pressure waves in water. Multiple spectra appear in each figure according to the value of the parameter α. Physically, the two extremes of the domain of α mean as follows: (a) $\alpha = 0$ corresponds to an infinite water depth of the reservoir, and (b) $\alpha = 1.00$ corresponds to a rigid reservoir bottom. Intermediate values correspond to different degrees of foundation rock acoustic impedance. Notice the resonant peaks at the natural frequencies of the impounded water, which grow without bound for $\alpha = 1.00$ (as in the case of a resonant elastic system without damping). The elasticity of the rock subbottom (assumed to extend to infinity) effectively acts within the dam-reservoir-subbottom system as an energy-dissipating mechanism.

Even a small amount of α-decrease from the vicinity of $\alpha \in (0.95,1.00)$ serves as a powerful moderator of maximum hydrodynamic responses. For frequency components of the excitation such that the ratio (ω/ω_1) smaller than about 0.50, the effect of α is negligible, and the system response remains relatively unaffected with respect to that for a rigid bottom. For frequency components of the excitation such that the ratio (ω/ω_1) lies between 0.50 and 0.80, the reduction in the system response is of intermediate magnitude, reaching up to 30% reduction at $(\omega/\omega_1) = 0.80$, for $\alpha = 0.20$, as compared to the corresponding dynamic magnification for $\alpha = 1.00$. The most dramatic attenuation of the system response occurs for frequency contents in the range for the ratio (ω/ω_1) from 0.80 to about 1.00, where the reduction reaches about 75% for $\alpha = 0.35$, for example, as compared to the dynamic magnification corresponding to α in the vicinity of 0.95. For $(\omega/\omega_1) > 1.00$, the effect of α on the system response in inconclusive due to oscillation according to the specific frequency content of the excitation.

4. EVALUATION

A seismic evaluation of the Folsom Dam and reservoir project has been performed (Hall, Woodson, and Nau 1989). The structure is located on the American River, 32 airline kilometers northeast of the city of Sacramento. The Folsom Project was designed and built by the Corps of Engineers during the period from 1948 to 1956 under the authority of the Flood Control Act of 1944 and the American River Basin Development Act of 1949. In May 1956, ownership was transferred to the U.S. Bureau of

Reclamation for operation and maintenance. The concrete gravity section (Fig 7) of the dam was designed with pseudo-static acceleration of 0.05 g acting upstream. Based on their studies of the horizonal ground acceleration recorded on an array of accelerometers normal to the Imperial Valley fault during the Imperial Valley earthquake of 1979, Bolt and Seed (1983) recommend the following ground motions:

Peak horizontal ground acceleration = 0.35 g

Peak horizontal ground velocity = 0.20 m/sec

Bracketed duration (0.05 g) = 16 sec

The seismic analyses of the critical nonoverflow monolith of the dam were conducted using the 2-D program, EACD-84 (Fenves and Chopra 1984). In this approach, the time history response of the dam subjected to the specified earthquake motions is determined with the simultaneous effects of dam-water interaction, dam-foundation rock interaction, and reservoir-bottom absorption included. Water compressibility is included in the analysis since the earthquake response of the concrete dam can be significantly affected by this factor. The foundation rock supporting the dam is idealized as a homogenous, isotropic, visco-elastic half plane. The dam monolith is idealized with an assemblage of four-node nonconforming planar finite elements. Dissipation of strain energy in the concrete is modeled with a constant hysteretic damping factor. A viscous damping ratio for all the natural vibration modes of the concrete dam on a rigid foundation with no reservoir corresponds to a constant hysteretic damping factor of twice the viscous damping ratio (Fenves and Chopra 1984).

The absorption nature of the reservoir subbottom is characterized by the wave reflection coefficient, α. The coefficient represents the dissipation of hydrodynamic pressure waves in the reservoir bottom and is modeled approximately by a boundary condition of the reservoir bottom which partially absorbs incident hydrodynamic pressure waves (Fenves and Chopra 1984). The wave reflection coefficient is defined as the ratio of the amplitude of the reflected hydrodynamic pressure wave to the amplitude of the vertically propagating pressure wave incident on the reservoir bottom. The material at the bottom of the reservoir determines the wave coefficient α, in the following equation:

$$\alpha = \frac{1-K}{1+K}$$

where

$K = \rho c / \rho_r c_r$

c = Velocity of pressure waves in water

ρ = Density of water

$c_r = \sqrt{E_r / \rho_r}$

E_r = Young's modulus of reservoir bottom material

ρ_r = Density of reservoir bottom material

For foundation rock module values of 40, 54.5, and 76 x 10^9N/m^2, the above equation leads to α values of 0.75, 0.79, and 0.82, respectively.

The pertinent stress analysis results are shown in Table 1. The greatest principal stresses occur for the case in which the foundation modulus and the reservoir-bottom coefficient are the largest. For this set of parameters, a maximum principal stress of 6 x 10^3N/m^2 occurs on the downstream face at an allocation of 22.5 meters from the crest. This region corresponds to that at which the vertical downstream face begins its transition to an inclined surface. The stress of 6 x 10^3 N/m^2 is greater that the recommended tensile strength of 5.8 x 10^3 N/m^2 for rich concrete. To investigate the depth to which possible cracking might penetrate, contours of envelope values of maximum principal stresses are shown in Fig 8. For the worse case, an area approximately 0.6 meters in depth on the downstream face is subjected to tensile stresses exceeding 4.8 x 10^3 N/m^2, the least tensile strength of the dam concrete. By including the effects of the reservoir-bottom absorption, it is reasonable to conclude that cracking will be quite limited in extent and depth of penetration into the monolith.

5. CONCLUSIONS

The effect of reservoir-subbottom energy absorption of the hydrodynamic loads on concrete dams subjected to large seismic ground motions may be substantial, particularly for excitation frequency contents in the range of $0.50 < (\omega/\omega_1) < 1.00$, where ω_1 is the fundamental frequency of the impounded reservoir. The measurement of the absorptive nature of the reservoir subbottom can be measured with different geophysical techniques. These techniques range from simple blasting cap techniques to very sophisticated waterborne measuring equipment. Analytical procedures are available from the simple 1-D wave propagation models to nonlinear constitutive models of partially saturated materials. What has not been determined is the needed degree of sophistication of the measurements or the analytical models. Further research needs to be performed to quantify the effect the spatial variation of the subbottom materials, as well as the geometry of the reservoir bottom, has on the hydrodynamic loads. These results will determine the needed parameters of an engineering model for the reservoir subbottom and the corresponding geophysical techniques.

6. AKNOWLEDGEMENTS

The research presented in this paper was sponsored by the Civil Works Direct-Allotted EQEN Program. We appreciate the cooperation of the authorities at the U. S. Army Engineer Waterways Experiment Station and the Office, Chief of Engineers, U. S. Army Corps of Engineers, that permitted us to prepare and present this paper for publication. Permission to publish this paper was granted by the Chief of Engineers.

7. REFERENCES

Hall, J. F., and Chopra, A. K. (1980). "Dynamic response of embankment, concrete-gravity, and arch dams including hydrodynamic interaction," Report No. UCB/EERC-80/39, Earthquake Engineering Research Center, University of California, Berkeley, CA.

Fenves, G., and Chopra, A. K. (1984). "EAGD-84: A computer program for earthquake analysis of concrete gravity dams," Report No. UCB/EERC-84-11, Earthquake Engineering Research Center, University of California, Berkeley, CA.

Fok, K. L., Hall, J. F., and Chopra, A. K. (1986). "EACD-3D: A computer program for three-dimensional earthquake analysis of concrete dams," Report No. UCB/EERC-86/09, Earthquake Engineering Research Center, University of California, Berkeley, CA.

Lotfi, V., Roesset, J. M., and Tassoulas, J. L. (1986). "A technique for the analysis of the response of dams to earthquakes," Earthquake Engineering and Structural Dynamics, Vol 15, pp 463-490.

Hall, R. L., Woodson, S. C., and Nau, J. M., (1987). "Seismic stability evaluation of Folsom Dam and reservoir project," Technical Report GL-87-14. U.S. Army Engineer Waterways Experiment Station, Vicksburg, MS.

Duron, Z. H., and Hall, J. F. (1988). "Experimental and finite element studies of the forced vibration response of the Morrow Point Dam," *Journal of Earthquake Engineering and Structural Dynamics*, Vol 16, pp1021-1039

Ghanatt, Y., Chen, H., Redpath, B. B., and Clough, R. W. (1993). "Experimental study of the Dongjiang Dam dam-water-foundation interaction," Technical Report QS93-03. Report to the National Science Foundation on Research conducted under the U. S. - China Protocol for Scientific and Technical Cooperation in Earthquake Studies, Quest Structures, Emeryville, CA.

Ghanaat, Y., and Redpath, B. B. (1995). "Measurements of reservoir-bottom reflection coefficient at seven concrete dam sites," Technical Report QS95-01, Report to the U.S.

Army Engineer Waterways Experiment Station and the Bureau of Reclamation, Quest Structures, Emeryville, CA.

Hunter, J.A., and Pullan, S.E. (1990). "A vertical array method for shallow seismic refraction survey of the Sea Floor," Geophysics, Vol 55, No 1, pp 92-96.

de Béjar, L. A. (1996). "Subbottom absorption coefficients for seismic analysis of concrete dams," *Proceedings from the First U.S. - Japan Workshop on Earthquake Engineering for Dams*, Vicksburg, MS.

Caulfield, D. C., Caulfield, D. D., and Yim, Y. (1985). "Shallow subbottom impedance structures using an iterative algorithm and empirical constraints," *Journal of the Canadian Society of Exploration Geophysicists*, 21(1), pp7-14.

Caulfield, D. D., and Yim, Y. (1983). "Prediction of shallow subbottom sediment acoustic impedance while estimating absorption and other losses," *Journal of the Canadian Society of Exploration Geophysicists*, 19(1), pp44-50.

Hamilton, E. L. (1980). "Geoacoustic modeling of the Sea Floor," *Journal of the Acoustical Society of America*, 68(5), pp1313-1340.

McGee, R.G., Ballard, R.F. Jr., and Caulfield, D.D. (1995). "A technique to assess the characteristics of bottom and subbottom marine sediments," Technical Report DRP-95-3, U.S. Army Engineer Waterways Experiment Station, Vicksburg, MS.

Telford, W.M., Geldart, L.P., Sheriff, R.E., and Keys, D.A. (1976). *Applied Geophysics*. Cambridge University Press, New York.

Westergaard, H.M. (1933). "Water pressures on dams during earthquakes," Trans. ASCE (98), pp 418-433.

Table 1. Effect of Reservoir Bottom Absorption

CASE	FOUND, MODULUS (10^9 N/m^2)	RESERVOIR BOTTOM REFLECTIVITY	MAXIMUM PRINCIPAL TENSILE STRESS (10^3 N/m^2) UPSTREAM FACE	DOWNSTREAM FACE
18	40.0	0.99	3433.71	3164.81
19		0.90	3013.12	2633.89
20		0.75	2585.63	2420.15
21	54.5	0.99	3833.62	4081.84
22		0.90	3213.07	3433.71
23		0.75	2744.21	3171.70
25	76.0	0.99	5619.43	6426.14
26		0.90	4716.18	5260.89
27		0.75	3819.83	4336.96

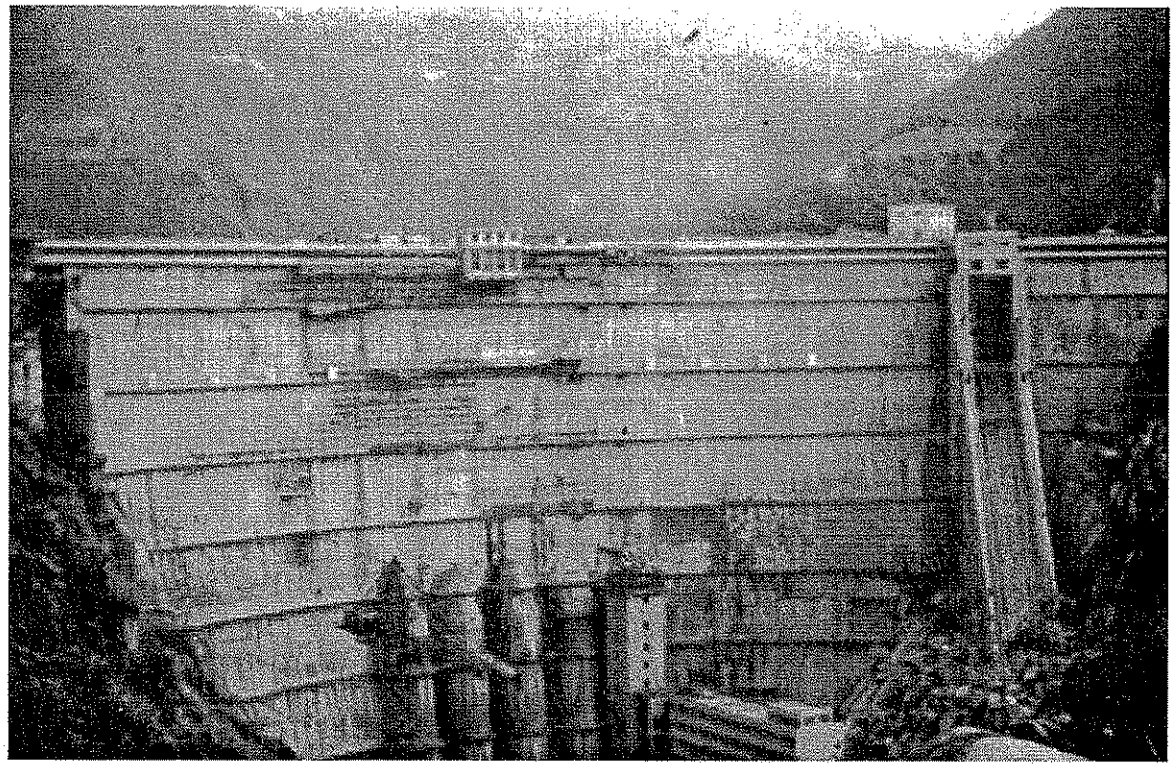

Figure 1. Dongjiang Dam

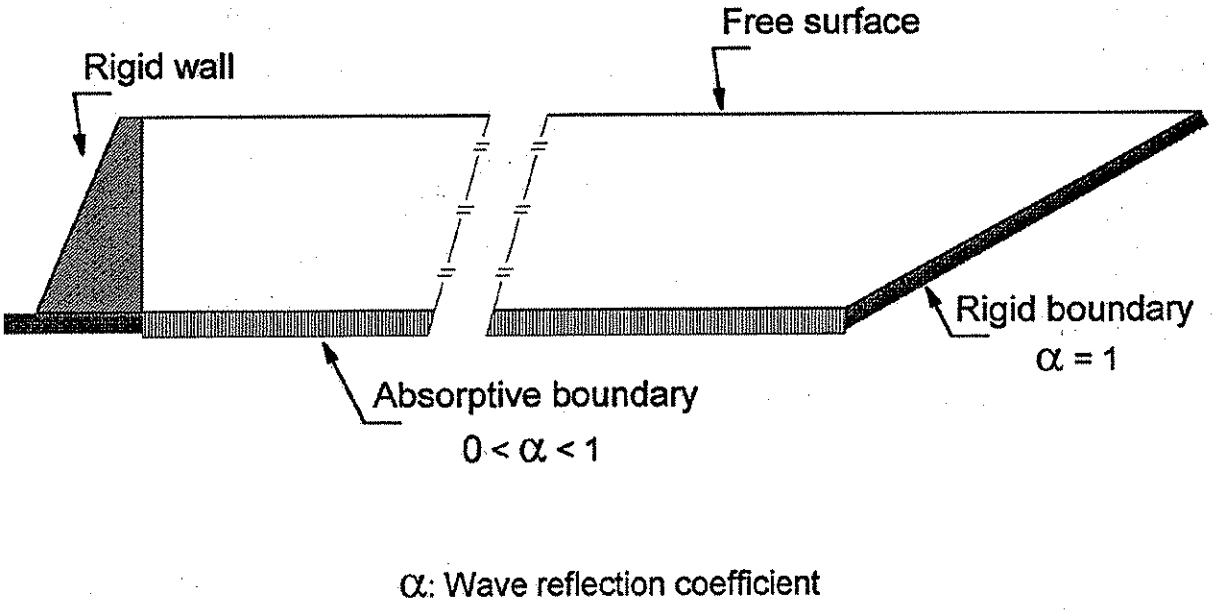

Figure 2. Trapezoidal Reservoir Incorporation of Bottom Absorption Characteristics

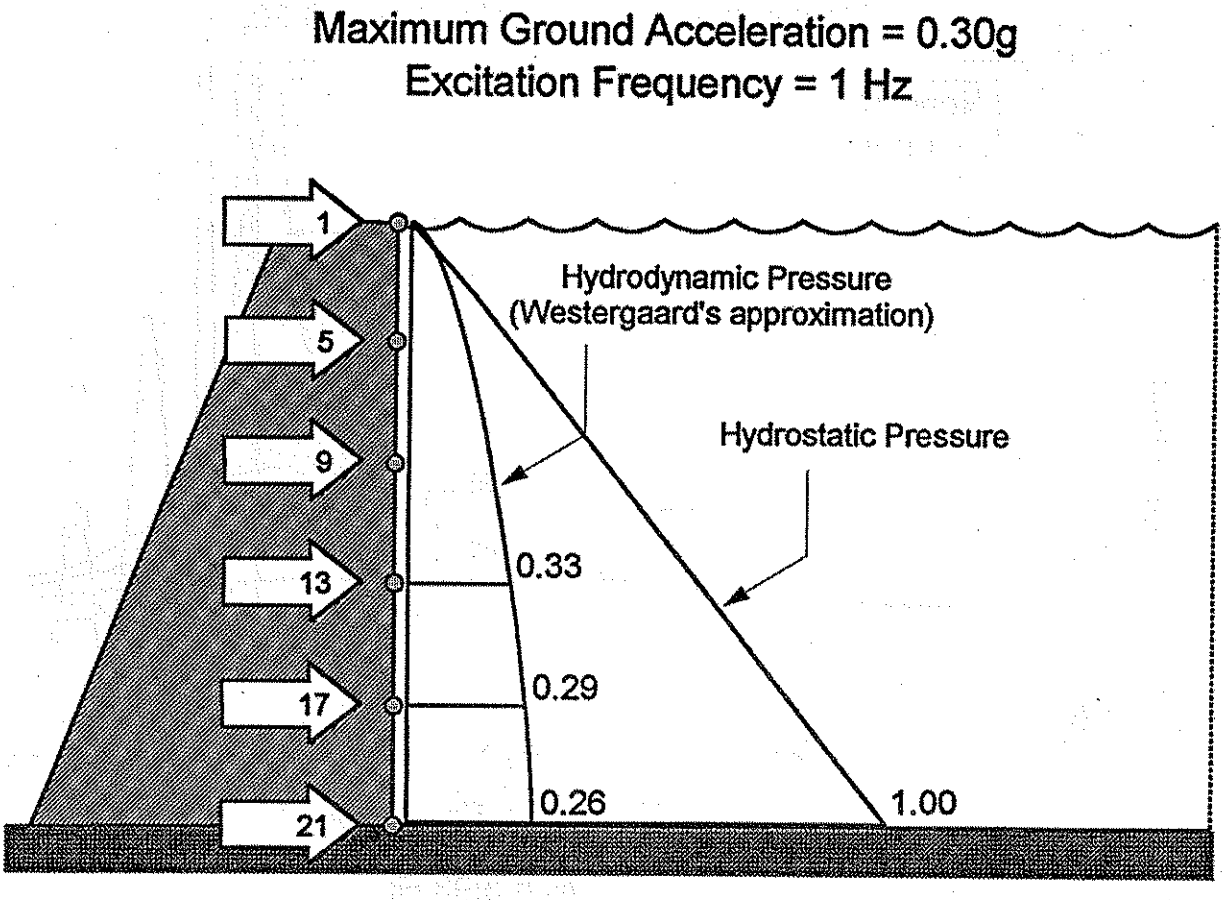

Figure 3. Trapezoidal Reservoir – Front Wall

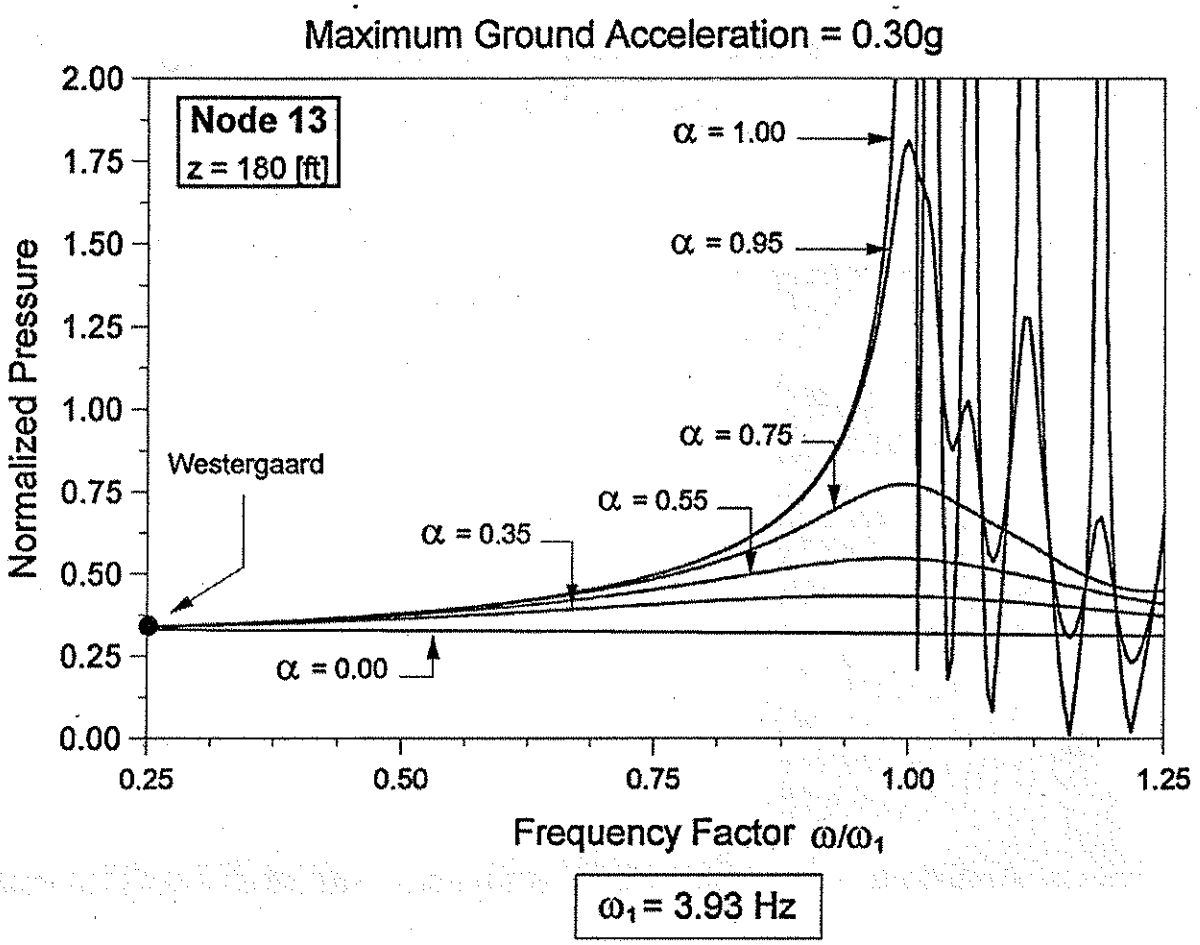

Figure 4. Trapezoidal Reservoir – 2D Analysis

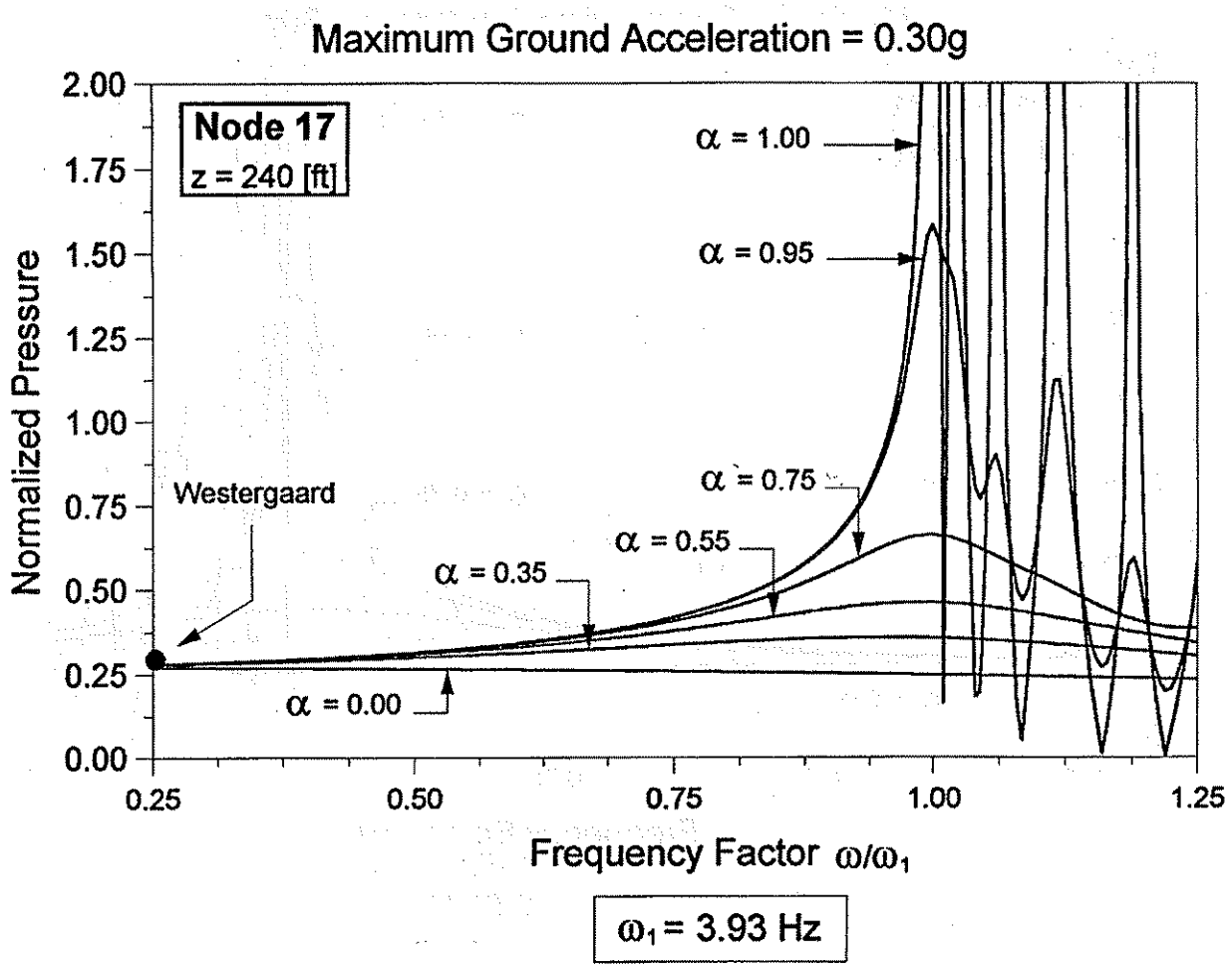

Figure 5. Trapezoidal Reservoir – 2D Analysis

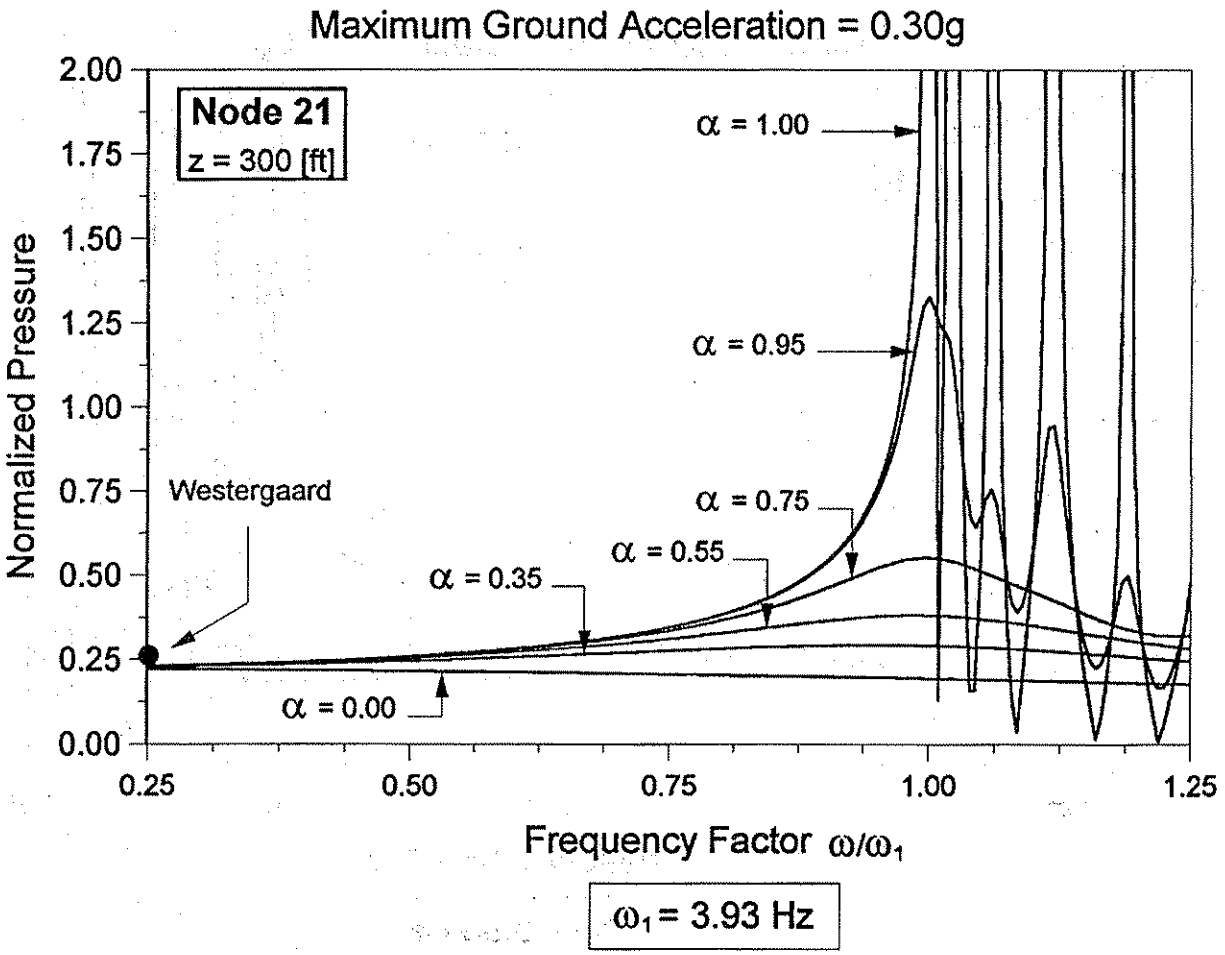

Figure 6. Trapezoidal Reservoir – 2D Analysis

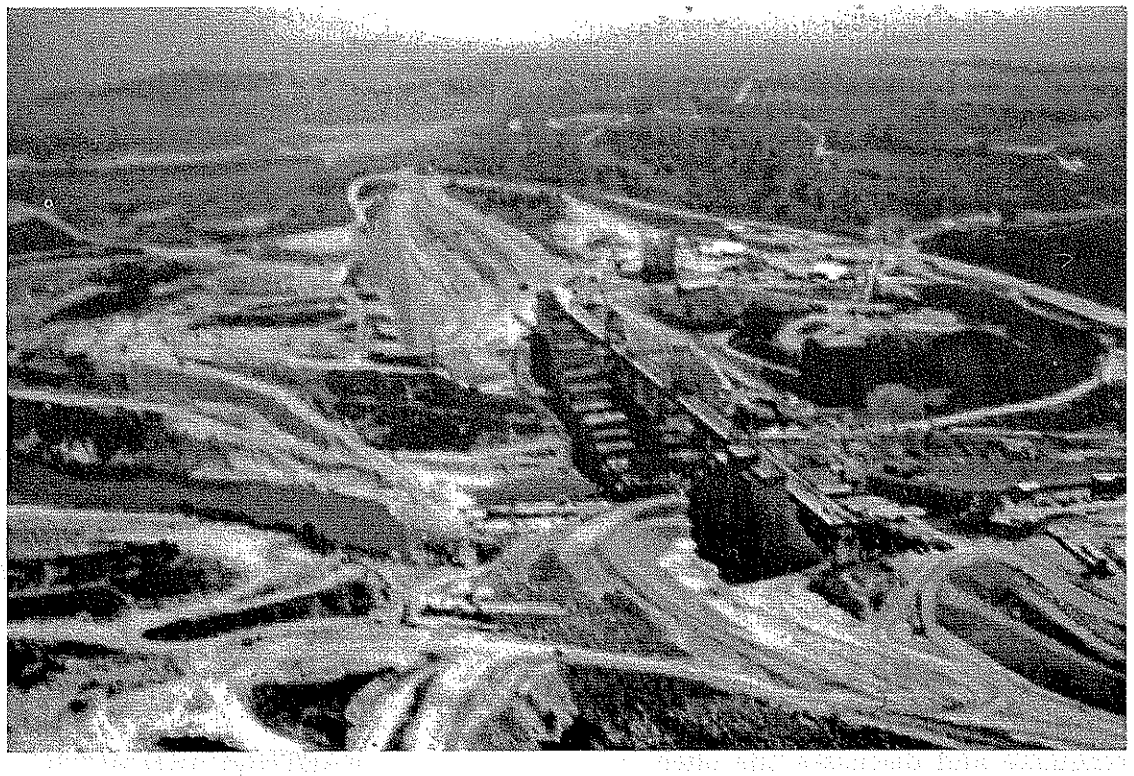

Figure 7. Folsom Dam

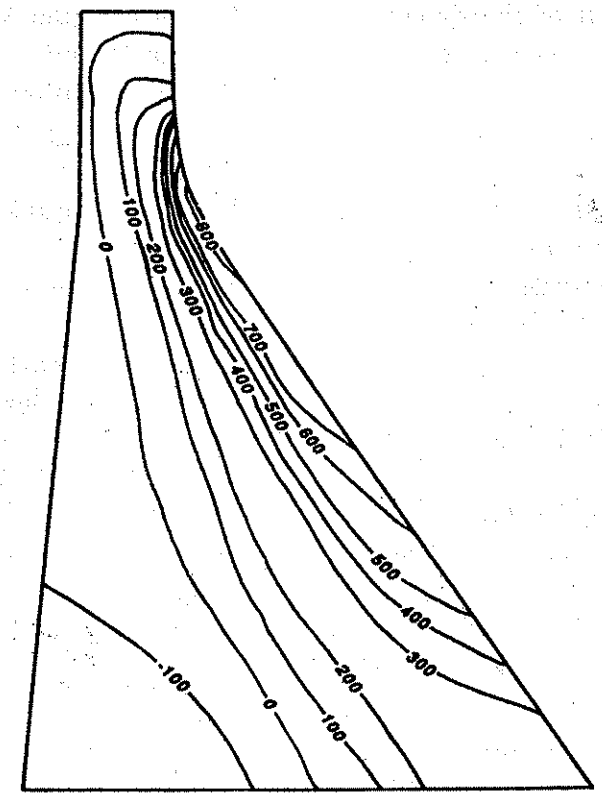

Figure 8. Maximum Principal Stress